PERGAMON

Journal of Structural Geology 23 (2001) 807–817

JOURNAL OF STRUCTURAL GEOLOGY

www.elsevier.nl/locate/jstrugeo

Measurement and interpretation of strain in the syntectonic Solís de Mataojo Granitic Complex, Uruguay

Pedro Oyhantçabal*, Adriana Heimann, Sara Miranda

Departamento de Geología, Facultad de Ciencias, Universidad de la República, Iguá 4225, 11 400 Montevideo, Uruguay

Received 10 January 2000; revised 5 October 2000; accepted 24 October 2000

Abstract

The Neoproterozoic Solís de Mataojo Granitic Complex is an intrusive body, elongate north–south, emplaced in the Sarandí del Yí–Arroyo Solís Grande Shear Zone. In the present work, a quantification of the magmatic strain has been made by analysis of fabric, enclave geometry and minor structures. Structural evidence indicates that deformation began in the magmatic state and continued through the subsolidus stage. The observed distribution of magmatic foliations and lineations, the fabric, the geometry of the enclaves and the late to post-magmatic structures, are related to a non-coaxial flattening regime that took place after the emplacement, and late in the magmatic history. These structures reveal that magmatic strain involved a shortening of the order of 80% with a simple shear component (γ) between 3 and 4.5. The solid-state deformation records an additional mean γ of 2.7.

1. Introduction

The Solís de Mataojo Granitic Complex (SMGC) is considered to be a syntectonic magmatic body, emplaced in a transcurrent shear zone (Oyhantçabal et al., 1993). The main purpose of this study is to characterize the deformation related to the magmatic state, using fabric and enclave data.

The analysis of magmatic fabric and enclave geometry supplies valuable quantitative and qualitative information about the strain regime and constitutes a tool to facilitate the understanding of the deformational history (Fernandez, 1987). Magmatic preferred orientation (fabric) is a result of the rotation of crystals under the effect of strain, and may be represented by a fabric ellipsoid whose vector radii are proportional to the cube root of the density of the markers or fabric intensity in each direction. The fabric is related to the strain path (Willis, 1977; Fernandez and Laporte, 1991) and in the case of pure or simple shear regimes, to finite strain (March, 1932; Fernandez, 1981, 1984).

Assuming that a magma contains a proportion of growing crystals of identical shape and with initial random distribution, that their shape can be approximated to that of an ellipsoidal particle, and that the crystals do not sink or interact, it is possible to establish a relationship between the fabric ellipsoid and the strain that produced this fabric. The relationship between fabric of passive markers and strain was established by March (1932) as follows:

$$D = r^3, \tag{1}$$

where D is the preferred orientation density of markers as a multiple of the homogeneous distribution, and r is the vector radius of the strain ellipsoid.

Fernandez (1981) established a generalization of this relationship for the case of rigid markers and pure shear strain history, as follows:

$$D = r^{3\kappa}, \tag{2}$$

$$D_{\max} = \lambda_1^{3\kappa/2} \ \text{(for prolate markers)}, \tag{3}$$

$$D_{\max} = \lambda_3^{3\kappa/2} \ \text{(for oblate markers)}, \tag{4}$$

where $D_{\max}$ is the maximum density of the fabric in multiples of uniform distribution, λ_1 and λ_3 are the quadratic extensions of the finite strain ellipsoid and κ is a shape parameter (established as $\kappa = (n^2 - 1)/(n^2 + 1)$, where n is the axial ratio of the marker).

The quadratic semiaxes of the fabric ellipsoid (Δ_1, Δ_2, Δ_3), can be obtained through the eigenvalues of a weighted orientation tensor (WOT), in which the matrix of the direction cosines is weighted by the density associated with each

* Corresponding author. Fax: +598-2-525-8617.

E-mail addresses: oyhantca@fcien.edu.uy (P. Oyhantçabal), adrianau@hotmail.com (A. Heimann).

0191-8141/01/$ - see front matter
PII: S0191-8141(00)00152-8

direction (Cobbold and Gapais, 1979). It is defined by:

$$\mathrm{WOT} = 3/N \begin{vmatrix} \Sigma r_i^2 x_i^2 & \Sigma r_i^2 x_i y_i & \Sigma r_i^2 x_i z_i \\ \Sigma r_i^2 x_i y_i & \Sigma r_i^2 y_i^2 & \Sigma r_i^2 y_i z_i \\ \Sigma r_i^2 x_i z_i & \Sigma r_i^2 y_i z_i & \Sigma r_i^2 z_i^2 \end{vmatrix} \quad (5)$$

where x_i, y_i and z_i are the direction cosines of the ith active marker, r_i is the cube root of the orientation density along the i direction, and N is the total number of markers. The quadratic extensions of the strain ellipsoid can then be estimated through the following relationships (Fernandez, 1981):

$$\lambda_1 = \Delta_1^{1/\kappa}\ \lambda_2 = \Delta_2^{1/\kappa}\ \lambda_3 = \Delta_3^{1/\kappa}\ \text{(for prolate markers)} \quad (6)$$

$$\lambda_3 = \Delta_1^{1/\kappa}\ \lambda_2 = \Delta_2^{1/\kappa}\ \lambda_1 = \Delta_3^{1/\kappa}\ \text{(for oblate markers)}. \quad (7)$$

In simple shear deformation, the motion of rigid markers in a viscous fluid is described by the following equations (Fernandez and Laporte, 1991):

$$\tan \phi_f = n \tan [(n\gamma)/(n^2 + 1) + \arctan ((\tan \phi_i)/n)] \quad (8)$$

$$\tan^2 \theta_f = \tan^2 \theta_i [(n^2 \cos^2 \phi_i + \sin^2 \phi_i)/(n^2 \cos^2 \phi_f + \sin^2 \phi_f)], \quad (9)$$

where n is the axial ratio of the particle, γ is the amount of shear, ϕ and θ define the orientation of the rotational axis of the particle (in radians, where θ is the polar angle with Y, and ϕ is the azimuth angle measured in the symmetry plane of the simple shear), and where the subscripts i and f refer to the initial and final angle, respectively. As a consequence of this relationship, the motion of an isolated particle is periodic and completes a full rotation when:

$$\gamma_{TM} = 4\pi/(1 - \kappa^2)^{\frac{1}{2}}. \quad (10)$$

Assuming that magma contains a proportion of growing crystals of identical shape and initial random distribution, that their shapes can be approximated by ellipsoids, and that the crystals do not sink or interact, the fabric evolves with increasing simple shear. The axis of maximum density Δ_1 rotates around the Y axis of the strain ellipsoid having an initial orientation of $-45°$, and reaches a maximum of intensity ($D_{max} = n^{-3}$) when the Δ_1 axis is parallel to the shear plane (for $\gamma = \pi/(1 - \kappa^2)^{\frac{1}{2}}$). The initial isotropic fabric is restored for a value of $\gamma = 2\pi/(1 - \kappa^2)^{\frac{1}{2}}$.

In a simple shear regime therefore, the magnitude of strain may be calculated from (a) the density *maximum* of the fabric (if $\gamma < \gamma_{TM}/2$), (b) the angular mismatch between two sub-fabrics of markers with different κ, or (c) the angle between the foliation plane and the shear plane (Fernandez and Laporte, 1991).

Fabrics associated with non-coaxial strain histories develop low (monoclinic) symmetry. The fabric axes of different mineral shape populations do not coincide (hetero-axial), though the relation between them allows the determination of the shear sense. In these regimes, a total quantification of strain from the fabric is not yet possible (Fernandez and Laporte, 1991).

Many of the assumptions stated above do not hold in real systems; for example, mechanical interactions between markers tend to slow down the rotation rate and thereby weaken the fabric intensity. For the case of simple shear, the cyclicity tends then to disappear (Ildefonse et al., 1992). For this reason, the fabric and the shape parameter κ, define a 'model strain ellipsoid', which represents the minimum strain ellipsoid responsible for the observed fabric (Fernandez and Fernández-Catuxo, 1997).

The measurement of comagmatic enclaves has been used by several authors to determine the strain within granitic bodies (Balk, 1937; Holder, 1979; Ramsay and Huber, 1983, pp. 81 and 205; Ramsay, 1989; Brun et al., 1990; Fowler and Paterson, 1997). If the viscosity contrast with the host magma is low, and if the initial shape of the enclaves is assumed to be spherical, the final shape of the enclaves provides an estimate of the finite strain ellipsoid. Many limitations appear when attempting a quantitative interpretation of data from individual enclaves. For example, if the initial shape is unknown, as well as both the absolute viscosity, and the viscosity contrast between enclave and matrix, the enclave shapes do not match that of the strain ellipsoid. However, the enclave distribution at the scale of the body supplies useful information about the strain history of the pluton (Fernandez, 1987; Guglielmo, 1993; Fowler and Paterson, 1997).

2. Geological framework

The Crystalline Basement of Uruguay has been divided into three major geotectonic units (Bossi and Campal, 1993; Fig. 1). At its western extremity, to the west of the Sarandí del Yí–Arroyo Solís Grande Shear Zone (SY–SG SZ), the Río de la Plata Craton (Paleoproterozoic age) is exposed. To the east of the SY–SG SZ, the Nico Pérez Terrane (Paleoproterozoic age) and the Dom Feliciano Belt, related to the Brasiliano Orogeny (Neoproterozoic to Cambrian), crop out.

The Río de la Plata Craton (Ferrando and Fernandez, 1971) is made up of large gneissic–granite areas, metamorphic belts of greenstone type, and intrusive granites. The Nico Pérez Terrane (Bossi and Campal, 1993) is composed of gneisses, amphibolites and quartzites affected by medium to high-grade metamorphism. The Dom Feliciano Belt is a transpressional orogen caused by an oblique continental collision (Fernandes et al., 1992), with extensive development of sinistral transcurrent shear zones. This belt has a general SSW–NNE structural trend and includes two low-grade metamorphic belts separated by a central mylonitized granitic area. Many of the syntectonic granite bodies recognized in the Dom Feliciano Belt (Uruguay) display strongly elongate geometries.

The SY–SG SZ, a large structure more than 600 km long

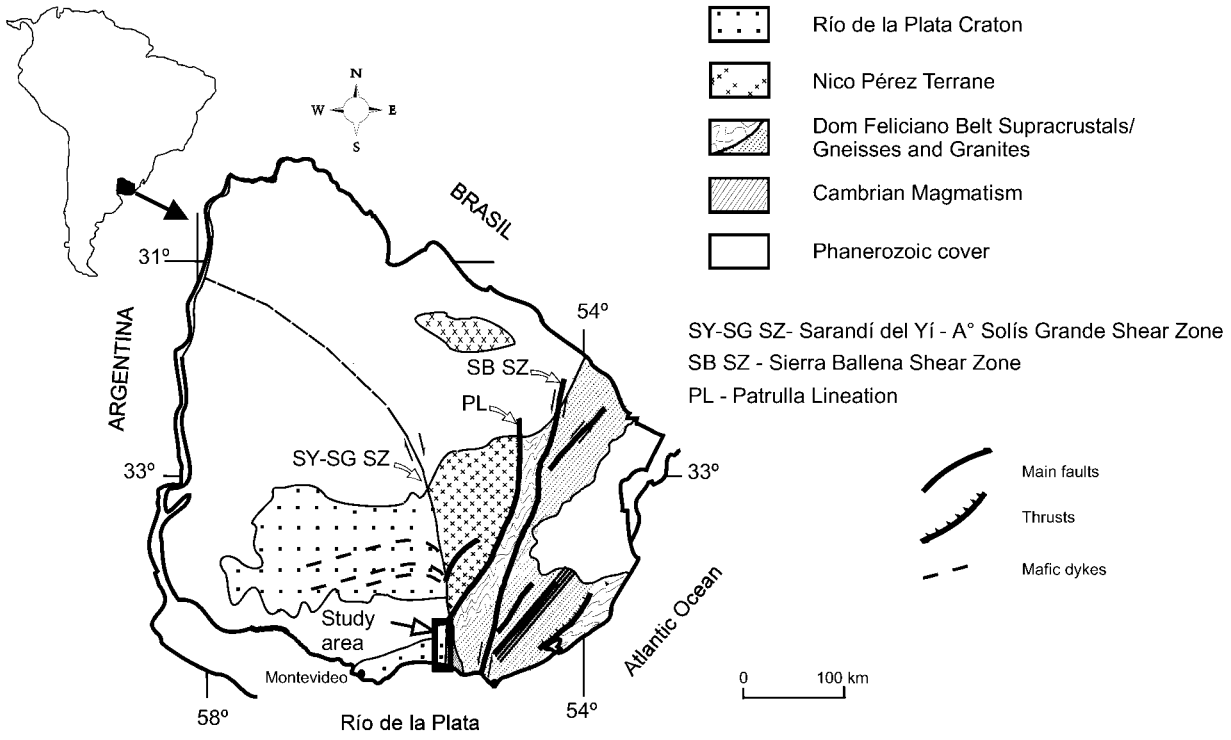

Fig. 1. Map showing Precambrian units of Uruguay and location of the study area.

and up to 15 km wide, constitutes one of the main tectonic features and controls the emplacement, geometry and deformation of the SMGC (Fig. 1). The SY–SG SZ was first recognized by Preciozzi et al. (1979), and Bossi and Campal (1991) demonstrated a dextral shear sense, recorded by drag folds in a mafic dyke swarm. According to the study of Oyhantçabal et al. (1993), this major shear zone underwent dextral movement after the intrusion of the dyke swarm dated around 1.88 Ga (Mazzuchelli et al., 1995), and suffered sinistral reactivation towards the end of the Brasiliano Cycle.

3. Solís de Mataojo Granitic Complex

The Neoproterozoic Solís de Mataojo Granitic Complex (SMGC), emplaced in the SY–SG SZ, is an elongate intrusive body of about 40 × 8 km, with an approximate north–south orientation (Fig. 2). Umpierre and Halpern (1971) have determined a Rb/Sr whole rock age 580 ± 15 Ma. To the north, Mesozoic sedimentary rocks of the Santa Lucía basin cover the pluton, to the south the Río de la Plata River interrupts it. Three main lithological types distributed in bands sub-parallel to the long axis of the intrusion are found: tonalites, porphyric granodiorites and granites (Fig. 2).

Tonalite occurs mainly in the western portion of the intrusion, forming a continuous band with a maximum width of 3 km. The texture is granular, with hypidiomorphic plagioclase (1–1.5 cm). The mineralogy consists of plagioclase with mean composition An_{30} (oligoclase–andesine), quartz, biotite, hornblende and occasional relicts of clinopyroxene. The most frequent accessories are sphene, zircon, apatite and allanite. There are abundant mafic enclaves with high aspect ratios.

Granodiorites occur in the central portion of the intrusion as discontinuous bands trending north–south. The texture is porphyritic, with megacrysts of microcline up to 7.5 cm in size and showing Carlsbad twinning, in a medium-grained granular matrix. The mineral composition is oligoclase (mean composition An_{25}), microcline, quartz, biotite and hornblende. The most frequent accessories are apatite, zircon, sphene and allanite. Enclaves with high aspect ratios are common.

Granite occurs in the central part of the intrusion. The texture is medium to fine equigranular allotriomorphic, frequently showing protomylonitic features. The mineralogy consists of quartz, oligoclase, microcline, biotite and muscovite with apatite and zircon as the most frequent accessories. Where strongly deformed, the granite shows abundant sericite.

Microgranitoid enclaves occur in tonalites and granodiorites, and are virtually absent in the granite. They display fine equigranular to microgranular texture with strong preferred orientation of plagioclase and ferromagnesian minerals. Their main minerals are plagioclase, biotite, hornblende, quartz and the accessories apatite, zircon and sphene. The composition of enclaves is quartz–dioritic in the case of tonalites, and tonalitic in the granodiorites.

The country rocks are mylonites which belong to the

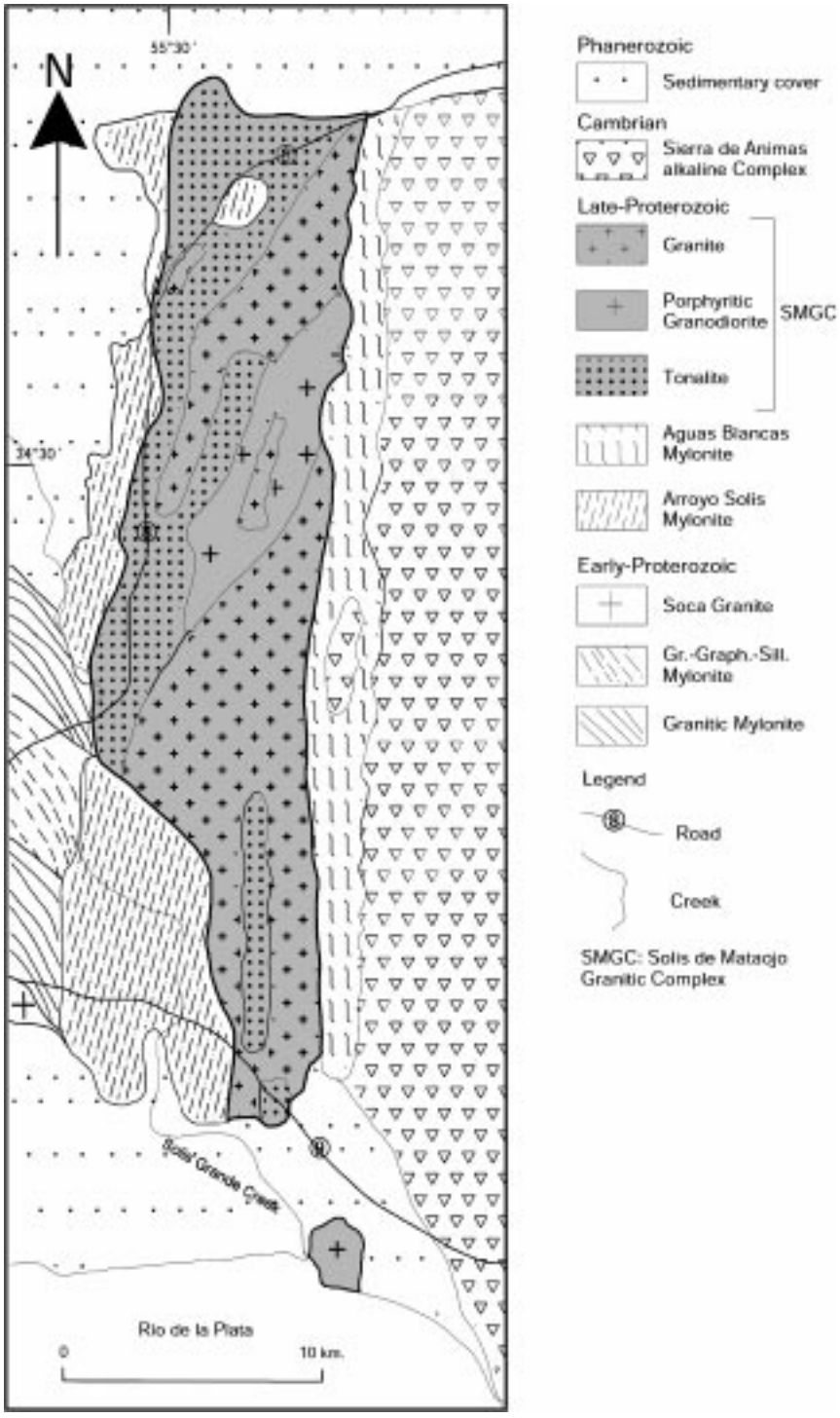

Fig. 2. Distribution of granitic facies of Solís de Mataojo Granitic Complex.

SY–SG SZ. To the west they are mainly made up of strongly deformed rocks with mylonitic foliation. Where the deformation is less intense, micaschists and amphibolites can be recognized. Muscovite–biotite–quartz–garnet–staurolite schists and plagioclase–hornblende–sphene amphibolites represent the protoliths. Ultramylonites rich in quartz and sericite, the protoliths of which have not been recognized, are also widespread.

To the east, the mapped unit referred to as the Aguas Blancas mylonites (Oyhantçabal et al., 1993) includes rocks derived from the strong deformation of the SMGC, as well as quartz–sericite–chlorite ultramylonites with unknown protoliths.

Within the SMGC, country rock xenoliths are common, and locally constitute large septa within which the SMGC has intruded.

4. Structural analysis

4.1. Magmatic lineation and foliation

The strike of the plane defined by the preferred orientation of (010) planes of feldspar megacrysts (magmatic foliation), and the preferred orientation of feldspar major axis (magmatic lineation), define three different zones: Northern, Central and Southern (Fig. 3). A magmatic foliation with mean strike of 040°, and a magmatic lineation with mean trend and plunge of 040°/30° characterize the Northern Zone. The Central Zone shows magmatic foliations with mean strike of 015–20°, and magmatic lineation of orientation 038°/10°. The Southern Zone shows north–south magmatic foliations sub-parallel to the boundaries of the intrusion. Associated magmatic lineations plunge variably, to the north or south between 0 and 35°.

It can be observed (Fig. 3) that the angle between the strike of the magmatic foliation and the contacts of the intrusion (ϕ angle), decreases from north to south, varying from 40° in the Northern Zone, to 20° in the Central Zone, and close to 0° in the southern part of the intrusion.

The angle ϕ decreases towards the contacts, suggesting a non-coaxial deformation regime during the emplacement and deformation of the intrusion (Blumenfeld and Bouchez, 1988).

The strain was estimated using the ϕ angle, assuming an ideal simple shear parallel to the intrusion boundaries, the magmatic foliation being taken as the major axis of the strain ellipse. The corresponding simple shear strain (γ) can be calculated from the relation:

$$\gamma = 2/\tan 2\phi$$

(March, 1932; Ramsay, 1980; Ramsay and Huber, 1983, p. 27).

For the Northern Zone this yields approximate γ values between 0.5 and 2. In the Southern Zone, the angles are much smaller and the apparent γ values varies between 2.4 and 4.1. The Central Zone yields intermediate γ values. Despite the structural evidence analyzed below, which indicates that the deformation regime was non-coaxial flattening so that a quantitative evaluation based on the ϕ angle is not possible, the approach to the evaluation of the deformation conducted analyzing variations of the ϕ angle indicates that the rotational component of the strain shows an increase from N to S.

4.2. Fabric of megacrysts

Two methods were used to carry out the fabric study depending on the quality of the outcrops: 3D measurements of the orientation of the (010) planes in K-feldspar megacrysts, or 2D measurements of the orientation of the intersection of K-feldspar megacrysts (010) plane with *XZ* and *YZ* principal planes. In the latter method, the 3D fabric ellipsoid was obtained from the 2D fabric ellipses using the FAB2D3D program (Fernandez and Fernández-Catuxo, 1997). This program finds, by iteration, the fabric axis of a population of markers that yields to 2D fabric ellipses, which match the observed ones in the real case. The program considers the probability that each marker cuts the planes *XZ* and *YZ*.

The fabric of K-feldspar megacrysts was studied at seven different sites (Fig. 3 and Table 1). For four of them (sites 4, 11, 15 and 21), the 3D fabric was measured directly, while in the other three sites the technique of measuring in two sections (*XZ* and *YZ*) was applied (sites 3, 7 and 20).

Three of the fabrics studied in 3D show low symmetry (sites 4, 11, 15, Fig. 4). At sites 4 and 11, the existence of a double maximum is also clear, although less defined in the diagram for site 15. The presence of double maxima in the sub-fabrics of K-feldspar megacrysts has been observed by several authors (Marre, 1986; Fernandez, 1984; Schulmann et al., 1997). Fernandez (1984) and Schulmann et al. (1997) have undertaken the numerical modelling of this phenomenon. Even though both authors suggest different orientation mechanisms, they both ascribe the presence of a double maximum to the joint effect of the markers' triaxial shape and the action of a simple shear regime. Considering the triaxial morphology of the markers and according to the results of numerical simulations performed by these authors, the fabric diagrams obtained for the SMGC are compatible with a non-coaxial component in the deformation.

In all sites studied, the maximum density values, counted within areas of 1/100 of the projection, range between 10 and 13%. In a simple shear regime, the maximum density value, for oblate markers, with axial ratio n, never exceeds n^{-3} (Fernandez, 1984). In the case of the SMGC, the K-feldspar megacrysts show a mean n value of 0.54 (Table 1), which implies a maximum theoretical value of $D_{\max\ \mathrm{simp}\ \mathrm{shear}} = 6.35$ (i.e. 0.54^{-3}). Then, the magmatic strain has been associated with a significant shortening component, necessary to explain the existence of $D_{\max}$ values higher than n^{-3}.

According to the criteria pointed out by Fernandez (1984), the $D = 1$ density curve of the fabric diagram, represents lines of no-finite elongation (since $\Lambda = D^{3/2}$ and $\lambda = \Lambda^{1/\kappa}$, then, if $D = 1$, λ must be equal to 1). In the SMGC, the closed shape of $D = 1$ curves in all the fabric diagrams (Fig. 4) correspond to a prolate fabric ellipsoid and then to an oblate strain ellipsoid, being also an evidence for an important shortening component.

The 3D fabric at site 21 shows unique maximum and axial type symmetry. This fabric allowed us to calculate a weighted orientation tensor (WOT) whose eigenvalues are $\Lambda_1 = 7.089$, $\Lambda_2 = 0.737$ and $\Lambda_3 = 0.191$. Considering the κ value $= -0.543$, these eigenvalues indicate a model strain ellipsoid with principal strains $X = 4.61$, $Y = 1.32$ and $Z = 0.16$, i.e. an oblate ellipsoid ($k_{\mathrm{Flinn}} = 0.35$), and a shortening greater than 80%. The density maximum of 13% observed at this site, also gives a value of $Z = 0.20$, which is consistent with the value obtained through the calculation with the WOT.

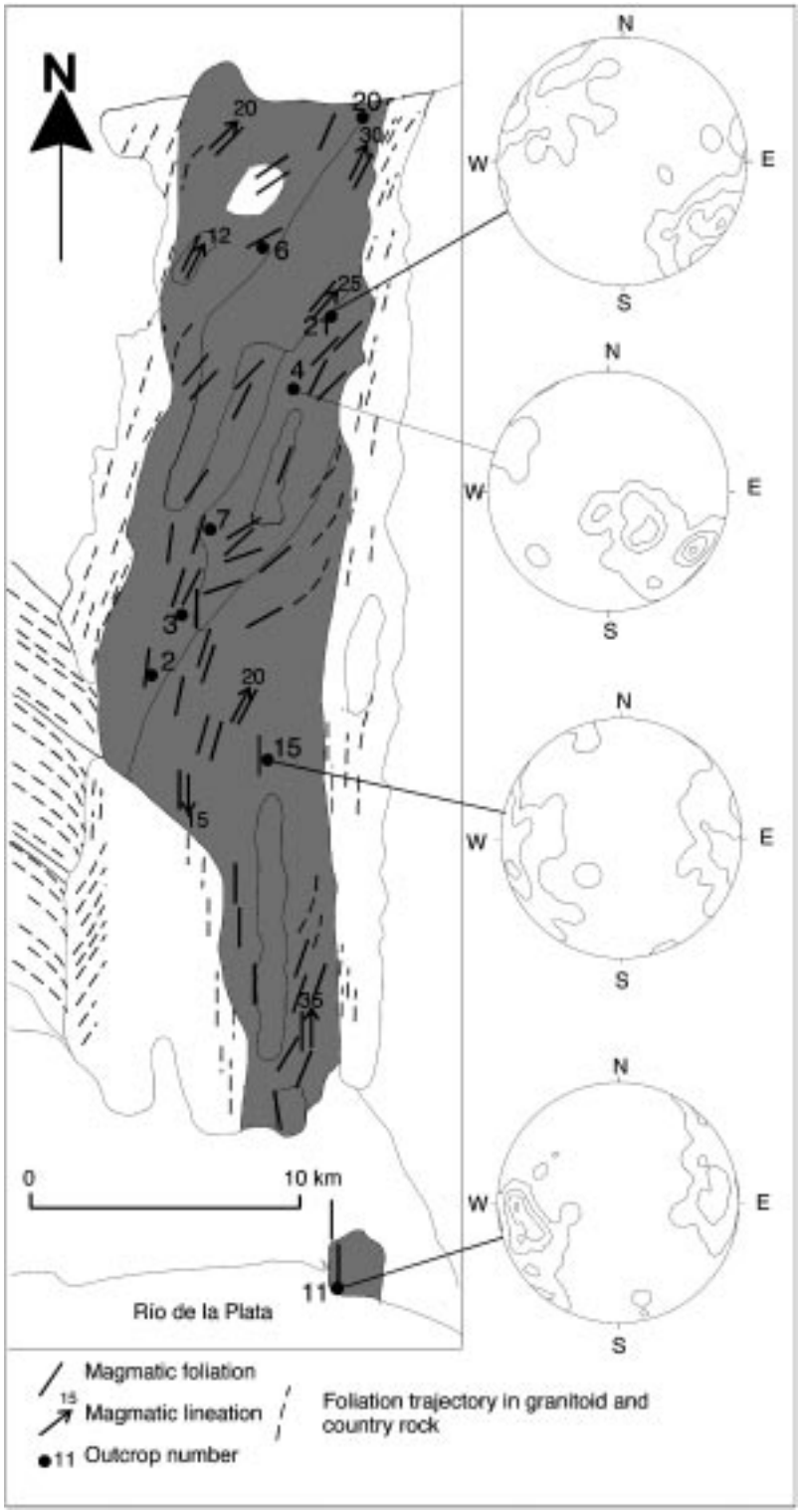

Fig. 3. Structural map showing distribution of magmatic foliation and lineation, and associated K-feldspar megacryst fabrics. Contour intervals 1, 4, 7 and 10%; D_{max} and N see Fig. 4.

The fabric in the Northern Zone, at site 20 (2D), which is also related to shortening as indicated by the shape of enclaves in the surroundings, provided a value of $Z = 0.21$, which corresponds to an oblate ellipsoid ($k_{Flinn} = 0.1$) with a shortening value (79%) very similar to that obtained at site 21.

The fabric at site 4 is heteroaxial, D_{max} is greater than n^{-3} and the fabric diagram shows two maxima, then this fabric

Table 1
(a) Numerical quantitative fabric and strain data: eigenvalue and density maximum (D_{max}) of fabric ellipsoid. (b) Strain parameters inferred from fabric and enclave shape. nd: no data

a

Site	Method	Aspect ratio (n)	κ	N or $N_{(XY)}/N_{(YZ)}$	D_{max} observed	Λ_1	Λ_2	Λ_3
3	2D	0.554	−0.53	60/58	–	1.96	1.03	0.49
4	3D	0.540	−0.54	100	11	5.41	0.98	0.19
7	2D	0.543	−0.55	99/50	–	1.74	1.02	0.56
11	3D	0.549	−0.54	100	11	3.97	1.54	0.16
15	3D	0.543	−0.54	101	10	3.6	1.73	0.16
20	2D	0.552	−0.54	94/85	–	2.34	0.76	0.56
21	3D	0.544	−0.54	100	13	7.09	0.74	0.19

b

Site	Fabric		X	Y	Z	$(X/Y) - 1$	$(Y/Z) - 1$	k_{Flinn}
	Symmetry	Maxima						
3	nd 2D		3.73	0.99	0.27	2.77	2.67	1.04
7	nd 2D		2.78	0.98	0.37	1.84	1.65	1.12
20	nd 2D		2.85	1.68	0.21	0.70	7.00	0.10
4	Low (triclinic)	Double	–	–	–	–	–	–
11	Low (triclinic)	Double	–	–	–	–	–	–
15	Low (triclinic)	Double	–	–	–	–	–	–
21	Axial	Single	4.61	1.32	0.16	2.49	7.25	0.35

Site	Enclaves	X	Y	Z	$(X/Y) - 1$	$(Y/Z) - 1$	k_{Flinn}
2	$N = 7$	3.13	2.86	0.11	0.09	25.00	0.004
6	$N = 10$	2.79	1.92	0.19	0.45	9.11	0.05

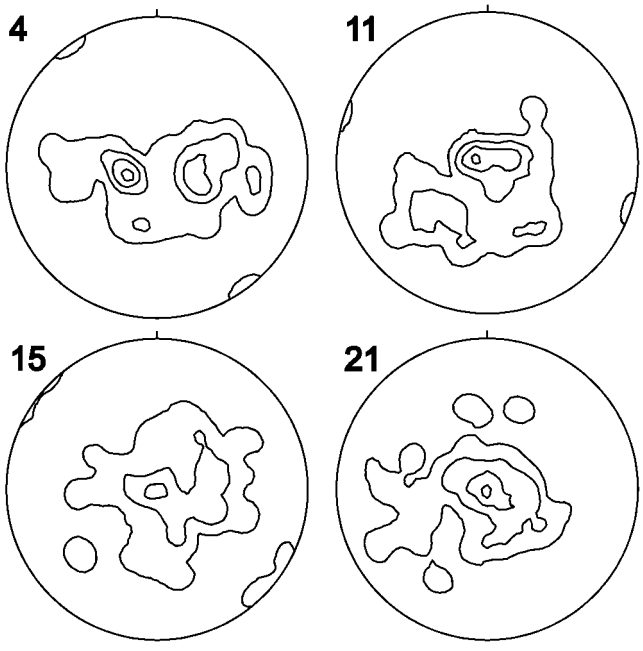

Fig. 4. K-feldspar megacryst fabrics from different sites of granodiorite facies in standard position (centered maximum). Contour intervals 1, 4, 7 and 10%; D_{max} in sites: 4 = 11%, 11 = 11%, 15 = 10% and 21 = 13%. N in sites: 4 = 104, 11 = 99, 15 = 100 and 21 = 101.

is related to non-coaxial shortening. At this site two populations of K-feldspar megacrysts with average κ of −0.448 and −0.702 are present (see Fig. 5) and the orientation in the XZ principal plane was studied for both subfabrics. The vector mean of the strike founded for these subfabrics is 013 and 022°, respectively, and the difference between them is 9°.

As stated by Ramberg (1975) and Fossen and Tikoff (1993), any progressive homogeneous strain can be expressed as a simultaneous combination of pure and simple shear. In order to estimate the simple shear component at site 4, a 2D numerical simulation using two populations of 180 markers uniformly distributed with aspect ratios $n = 2.39$ and 1.62 ($\kappa = -0.448$ and -0.702), was conducted. The equation of Ghosh and Ramberg (1976) was used to estimate the motion of the markers. This equation describes the angular velocity ($\dot{\phi}$) of a rigid ellipse in a Newtonian matrix as:

$$\dot{\phi} = \frac{\dot{\gamma}}{n^2 + 1}(n^2 \sin^2\phi + \cos^2\phi) + \frac{n^2 - 1}{n^2 + 1}\dot{\varepsilon}\sin 2\phi \qquad (11)$$

where n is the aspect ratio of the elliptical rigid marker, ϕ is the angle between the normal to the shear plane (y-axis) and the major axis of the elliptical rigid marker, $\dot{\gamma}$ is the simple shear strain rate and $\dot{\varepsilon}$ the compressional strain rate. The evolution of the angle between Λ_1 axis of the fabric ellipse

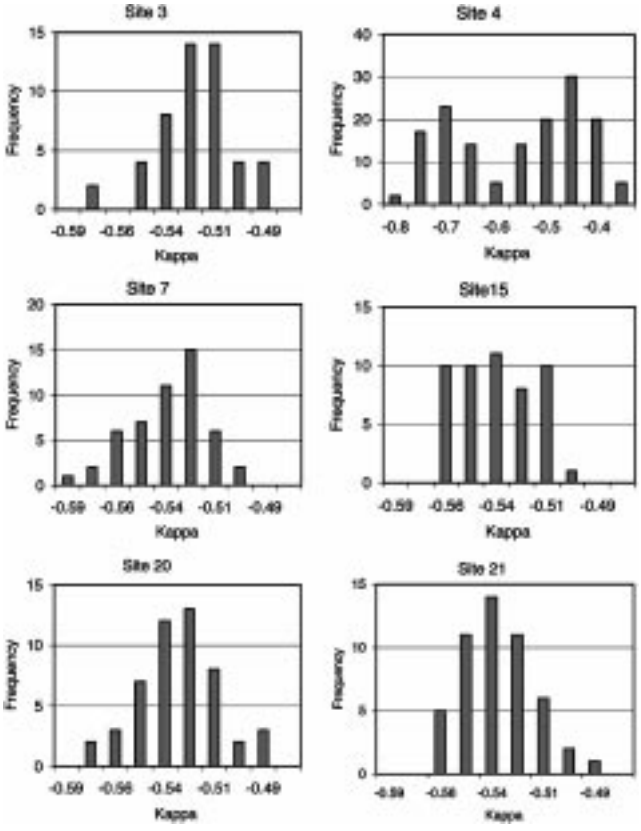

Fig. 5. Histograms of κ values. Number of measured megacrysts: sites 3, 7, 15, 20 and 21 = 50, site 4 = 100.

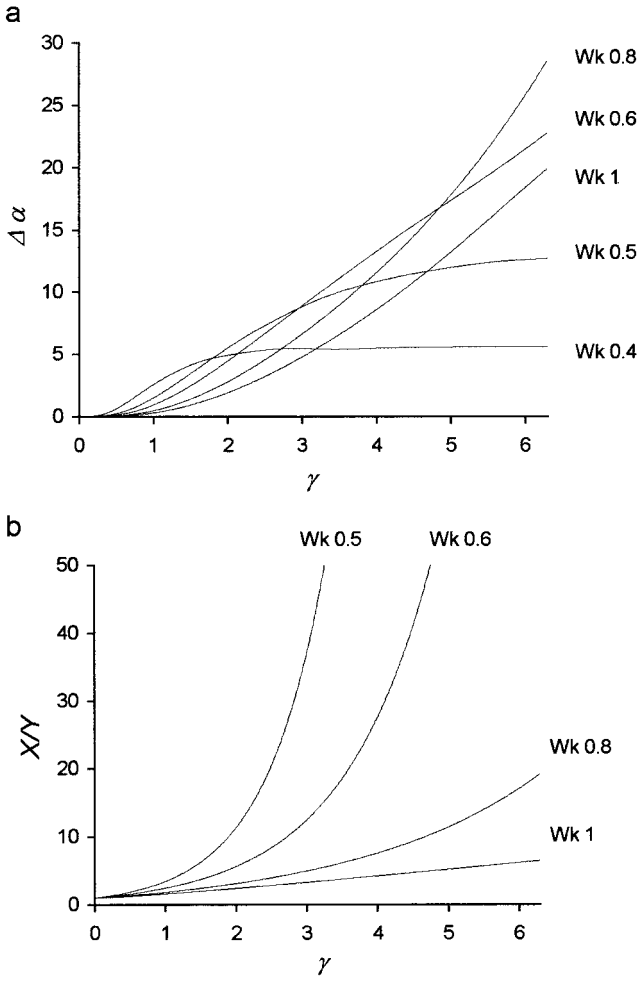

Fig. 6. (a) Evolution of the difference of the orientation ($\Delta\alpha$) of the major axis Λ_1 of the fabric ellipsoid between two populations of markers with different aspect ratios ($n = 2.39$ and 1.62), by different simultaneous combinations of simple shear and pure shear (Wk). (b) Variation in ellipticity (X/Y) for different Wk with progressive deformation.

and the y-axis (α angle), and the difference between both populations ($\Delta\alpha$) versus γ is shown in Fig. 6a.

The simulation suggests that the kinematic vorticity number, Wk (Truesdell, 1953), an index of non-coaxiality, was greater than 0.4, in order to reach the observed mismatch (see Fig. 6a). This number was probably bigger than 0.6, otherwise the aspect ratio of the strain ellipse needs to be extremely large (see Fig. 6b).

The mismatch between both sub fabrics studied ($\Delta\alpha = 9°$), also indicates an approximate value of γ for the simple shear component of the deformation between 3 and 4.5.

Such a γ value is consistent with the simulations by Fernandez (1984), using triaxial markers with axial ratios $a/b = b/c = 1.5$ ($\kappa = c/(ab)^{\frac{1}{2}} = -0.546$). This author found that double maxima appearance occurs when γ values exceed 3. In the SMGC such double maxima are observed in sites 4, 11 and 15. The scattering displayed by the fabric ellipsoids in a $(\Lambda_1/\Lambda_2)^{\frac{1}{2}}$ versus $(\Lambda_2/\Lambda_3)^{\frac{1}{2}}$ diagram (Fig. 7b) is similar to the trend found by Fernandez and Laporte (1991) during the simulation of the fabric evolution in a non-coaxial shortening regime with increasing amount of shear.

In the northern part of the Massif, where shortening predominates and the angles between foliation and granite boundaries are higher, the existence of an inferred intrusive boundary towards the NW, with a 045° strike, might have allowed the development of the observed shortening. This structural direction, which is coincident with the border of a Mesozoic basin developed to the north, may have constituted a previous discontinuity reactivated towards the Mesozoic during the extension of this basin.

4.3. Geometry of the enclaves

The shapes of xenoliths (corresponding to fragments of country rock) do not show evidence of strain, whereas the shapes of the co-magmatic enclaves do.

The enclaves considered in this study have quartz–dioritic composition, and are enclosed in a tonalitic host, which allows us to infer low viscosity contrast and, consequently, that the shape of enclaves will be approximately that of the finite strain ellipsoid. However, the primary shape question remains.

The methodology used to measure the enclaves consisted

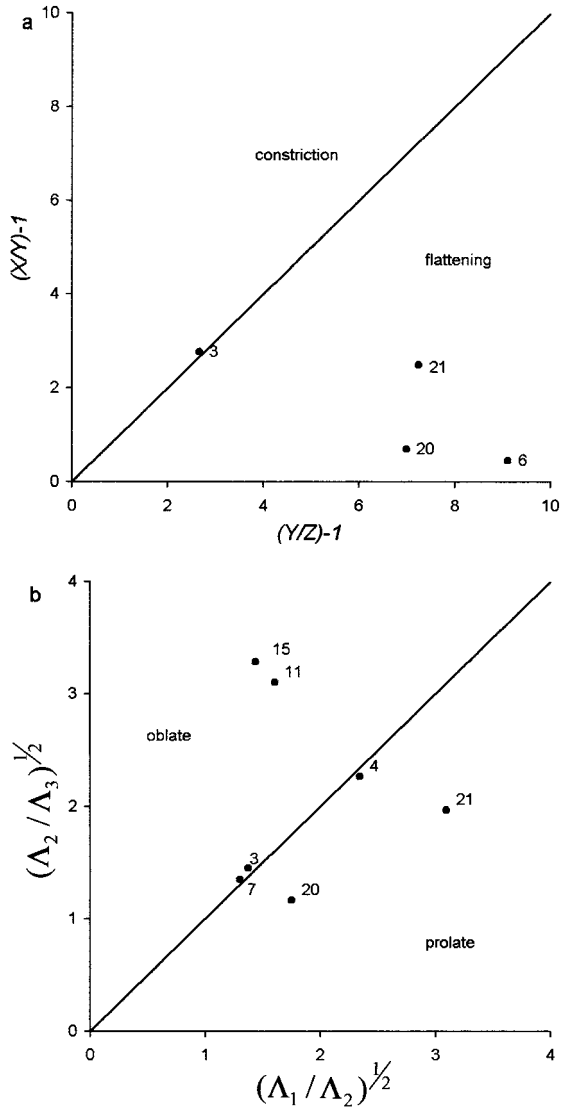

Fig. 7. Shape of strain ellipsoids in a Flinn diagram (a) and shape of fabric ellipsoids in a $(\Lambda_1/\Lambda_2)^{\frac{1}{2}}$ versus $(\Lambda_2/\Lambda_3)^{\frac{1}{2}}$ diagram (b) for different sites of the SolÍs de Mataojo Granitic Complex.

of recording their axial ratios in sections perpendicular to foliation and lineation (*YZ* sections), and perpendicular to the magmatic foliation and parallel to the lineation (*XZ* sections) for different enclaves at the same outcrop. Where measurements in both planes were possible, the values were integrated in a common model ellipsoid using the ratios *Y*/*Z*, *X*/*Z* and the constant volume assumption ($XYZ = 1$).

Only two outcrops (sites 6 and 2) yielded information about both (*Y*/*Z* and *X*/*Z*) ratios.

In the Northern Zone, the average axial ratio obtained in *XY* sections was 1.45, while it was 10.1 in *YZ* sections, which results in values of $X = 2.79$, $Y = 1.92$ and $Z = 0.19$ (site 6). The corresponding k_{Flinn} value is 0.05 showing a shortening greater than 80%. The axial ratio dispersions calculated from the measure of *XZ* and *YZ* sections of enclaves from site 6, in which an ellipsoid could be integrated, are shown in Fig. 6 and Table 1. This average $Z = 0.19$ allows the prediction (using the relation $D_{\max} = Z^{3\kappa}$) of a theoretical maximum density of 15% for the fabric of megacrysts with $\kappa = -0.543$. This value is in good agreement with the $D_{\max}$ of 13%, observed in the fabric in adjacent outcrops (site 21, Fig. 4).

The average axial ratio registered in the Central Zone was 1.09 in *XY* sections, and 26.0 in *XZ* sections (site 2). These ratios result in values of $X = 3.13$, $Y = 2.86$ and $Z = 0.11$. The k_{Flinn} is 0.004, revealing shortening close to 90%.

In summary, although the information is compiled from different sites, in both cases, the deformation shown by the enclaves is consistent with the data obtained from the fabrics with axial symmetry (Table 1).

4.4. Late magmatic structures

In the SMGC, the following features can be observed:

- Aplitic and pegmatitic dykes with ptygmatic-like folds, with fold axial planes approximately parallel to the foliation. According to the method described by Ramsay and Huber (1983, pp. 100–103), they indicate a shortening close to 60%. They are considered to be indicators of shortening during the late magmatic state (Fig. 8a).
- Aplitic and pegmatitic dykes displaced by sinistral shear belts (Fig. 8b). These are rectilinear dykes related to extension, parallel to the *X* axis, of the finite strain ellipsoid during late-magmatic stages. They frequently show sinistral displacements, associated with decimeter-scale shear zones developed during the late to post-magmatic state, similar as those described by Vauchez (1987). The displacement value measured in the field, and the width of the sheared belt, allowed us to estimate locally values of γ (see Ramsay and Huber, 1983, pp. 44–52), accumulated during the sub-solidus stage. The calculated average γ value for the studied shear zones displacing dykes is 2.70.

4.5. Post-magmatic structures

The temperatures assigned for microstructural features are based on Passchier and Trouw (1996) and Gapais (1989). In the SMGC, the following microstructural features, described in terms of progressive cooling during deformation, are observed:

- The presence of basal quartz subgrains generated by c-slip, developing grains with positive elongation subparallel to the foliation. This evidence shows that a solid-state deformation occurred at high temperatures close to the solidus of the granites (700–800°C).
- Myrmekites (indicating temperatures above 500–550°).
- Uncommon development of quartz subgrains, with formation of fine-grained aggregates (mortar texture) as well as grains with sutured boundaries; polyhedral grains

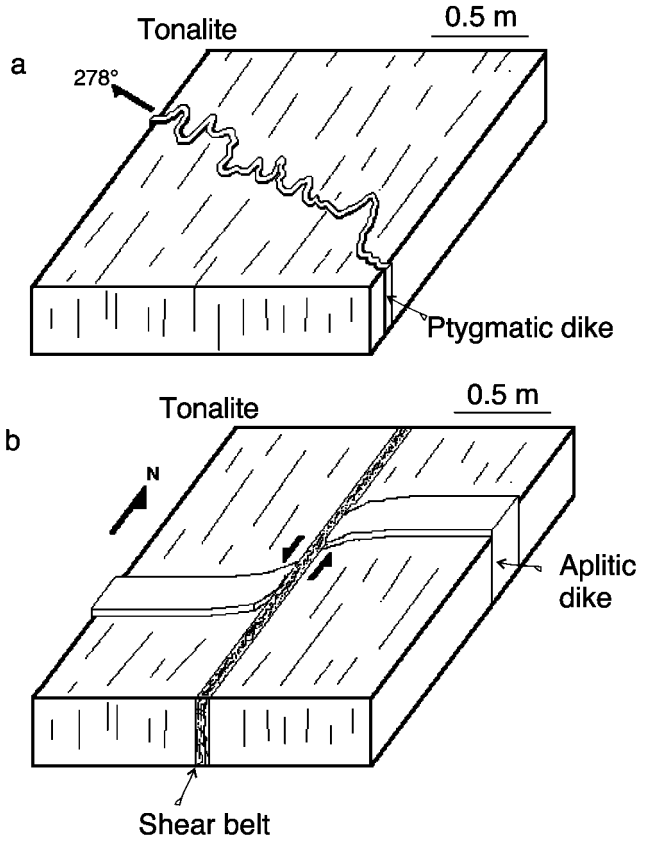

Fig. 8. Schematic representation of late magmatic structures: (a) Aplitic dyke with quasi-ptygmatic folds; (b) Aplitic dyke displaced by sinistral shear belts.

(mosaic texture) are uncommon. These structures indicate an increase of deformation in the solid state.

- Core and mantle structures of fine-grained aggregates of quartz, surrounding coarser quartz grains.
- Ribbon quartz.
- Kink bands in biotite and muscovite, and twisted twins in plagioclase, with preferred orientation expressing a later plastic deformation (300–400°C).
- Recrystallization of quartz, mica, chlorite and calcite in necks of boudined feldspar, which indicates flattening in the solid state and dynamic recrystallization under greenschist facies conditions (300–400°C).
- Fractures in feldspars, filled by fine-grained quartz and calcite aggregates, revealing brittle behaviour under low temperature conditions (below 300°C).
- Fractured amphiboles, showing further evidence of deformation in a strong mineral.

4.6. Kinematic indicators

The magmatic fabric has preserved indicators of sinistral sense of shear. Analysis of the preferred orientation of feldspar megacrysts, by dividing them into two sub-populations with different axial ratio ranges, shows that those with a small ratio form a lower angle (α) with the shear plane (see Section 4.2). The observed pattern is compatible with a sinistral shear sense (Fig. 5).

The fabric diagram of site 11 shows asymmetric $D = 1$ curves with respect to its maximum, which, applying the criterion defined by Fernandez and Laporte (1991), reveals sinistral sense.

Numerous plagioclase crystals in tonalite of the SMGC show a tilling (Blumenfeld and Bouchez, 1988), which indicates a sinistral sense of shear. S–C structures (Berthé et al., 1979) also reveal a sinistral shear sense in the post-magmatic stage.

5. Conclusions

The deformation observed in the Solís de Mataojo Granitic Complex began in the magmatic state and continued in the sub-solidus stage, and is quite heterogeneous.

Deformation in the magmatic state is expressed by the presence of the following features:

- Strong shape preferred orientation of feldspar megacrysts.
- High axial ratio of enclaves, with preservation of magmatic texture.
- Parallel orientation of enclaves and magmatic foliation.

A large part of the sub-solidus deformation observed in the SMGC took place at high temperatures, close to the granite solidus (transition magmatic-solid-state flow), with the presence of c-slip providing evidence that solid-state deformation occurred at about 600–800°C under hydrated conditions. Additionally, it is possible to observe a subordinate deformation developed at lower temperatures (greenschist facies).

Sub-solidus stage deformation resulted from the continuity of the Sarandí del Yí–Arroyo Solís Grande Shear Zone activity after magma solidification. It is especially marked by intragranitic shear belts ranging in width from a few centimeters to a few hundreds of meters.

The observed distribution of magmatic foliations and lineations, the fabric, the shape of the enclaves and the late-postmagmatic structures, are all related to a non-coaxial flattening regime, that took place after the emplacement and late in the magmatic history.

The magmatic strain recorded in the SMGC reveals local shortening of the order of 80%, with a rotational component γ of between 3 and 4.5. Considering an average width for the pluton of 8 km, this average value of γ implies an estimated displacement, recorded in the fabric, of 30 km. The overall shape of the intrusion should be ascribed to emplacement mechanism and does not result only from strain.

Intragranitic sub-solidus shear belts registered a mean γ of 2.7. From several cross-sections through the pluton, a mean proportion of 20% of these shear belts were found, indicating between 4 and 5 km bulk displacement.

Total sinistral displacement recorded in the SMGC under

magmatic and solid-state conditions is approximately 40 km.

The distribution of syn-magmatic structural characteristics for the pluton indicates that the strain regime had an important rotational component in the Southern Zone, while in the Northern Zone coaxial flattening predominated because of the existence of a limit perpendicular to the main compressive stress (σ_1), which controlled the strain locally.

Acknowledgements

We are indebted to Angel N. Fernandez for orientation, for help with the fieldwork and for significant improvements to our initial paper. We thank Stephen Amor for substantial improvements to our English and to Juan Ledesma for constructive suggestions during the preparation of the paper. Thorough reviews by D. Gapais and J.V. Smith helped improve and clarify the manuscript. We would like also to thank S.R. Paterson and S. Molyneux for the reviews and detailed comments on an earlier version of the manuscript.

References

Balk, R., 1937. Structural behaviour of igneous rocks. Memoirs of the Geological Society, America, 5.

Berthé, D., Choukroune, P., Jegouzo, P., 1979. Orthogneiss, mylonites and non-coaxial deformation of granites: the example of the South Armorican shear zone. Journal of Structural Geology 1, 31–42.

Blumenfeld, P., Bouchez, J.L., 1988. Shear criteria in granite and migmatite deformed in the magmatic and solid states. Journal of Structural Geology 10, 361–372.

Bossi, J., Campal, N., 1991. Granitos negros filoneanos del Uruguay. Facultad de Agronomía, Montevideo.

Bossi, J., Campal, N., 1993. El Cinturón Cuchilla de Dionisio: evento Brasiliano uruguayo. 1er Simposio Internacional del Neo-proterozoico Cámbrico de la Cuenca del Plata, 43–56.

Brun, J.P., Gapais, D., Cogne, G.P., 1990. The Flamanville Granite Northwest France: an unequivocal example of a syntectonically expanding pluton. Geological Journal 25, 271–286.

Cobbold, P., Gapais, D., 1979. Specification of fabric shapes using an eigenvalue method: Discussion. Geological Society of America Bulletin 90, 310–312.

Fernandes, L., Tommasi, A., Porcher, C., 1992. Deformation patterns in the southern Brasiliano branch of the Dom Feliciano Belt: a reappraisal. Journal of South American Earth Sciences 5, 75–96.

Fernandez, A., 1981. Une généralisation de modèle de March applicable à l'analyse des orientations préférentielles de forme issues de la déformation coaxiale dans les roches éruptives. Compte Rendu Academie des Sciences de Paris, 294 II, pp. 1091–1094.

Fernandez, A., 1984. Etude théorique et expérimentale du développement de la fabrique dans les roches magmatiques. Aplication à l'étude structurale des granitoides. Ph.D. thesis, University of Clermont Ferrand II.

Fernandez, A., 1987. Structural petrology and intrusion strain analysis. Revista Brasilera de Geociências 17, 372–381.

Fernandez, A., Fernández-Catuxo, J., 1997. 3D Biotite shape fabric experiments under simple shear strain. In: Bouchez, J.L., Hutton, D.H.W., Stephens, W.E. (Eds.). Granite: from Segregation of Melt to Emplacement Fabrics. Kluwer Academic Publishers, Netherlands, pp. 145–157.

Fernandez, A., Laporte, D., 1991. Significance of low symmetry in magmatic rocks. Journal of Structural Geology 13, 337–347.

Ferrando, L.H., Fernandez, A., 1971. Esquema tectónico-cronoestratigráfico del Predevoniano en el Uruguay. Congreso Brasileiro de GeologÍa, 25. San Pablo, Anais 1, pp. 199–210.

Fossen, H., Tikoff, B., 1993. The deformation matrix for simultaneous simple shearing, pure shearing and volume change, and its applications to transpression–transtension tectonics. Journal of Structural Geology 15, 413–422.

Fowler, T.K., Paterson, S.R., 1997. Timing and nature of magmatic fabrics from structural relations around stopped blocks. Journal of Structural Geology 19, 209–224.

Gapais, D., 1989. Shear structures within deformed granites: mechanical and thermal indicators. Geology 17, 1144–1147.

Ghosh, S.K., Ramberg, H., 1976. Reorientation of inclusions by combination of pure shear and simple shear. Tectonophysics 34, 1–70.

Guglielmo Jr, G., 1993. Magmatic strains and foliation triple points of the Merrimac plutons, northern Sierra Nevada, California: implications for pluton emplacement and timing of subduction. Journal of Structural Geology 15, 177–189.

Holder, M.T., 1979. An emplacement mechanism for post-tectonic granites and its implications for their geochemical features. In: Atherton, M.P., Tarney, J. (Eds.). Origin of Granite Batholiths—Geochemical Evidences. Shiva Publishing, Orpington, pp. 116–128.

Ildefonse, B., Launeau, P., Bouchez, J., Fernandez, A., 1992. Effect of mechanical interactions on the development of shape preferred orientations: a two-dimensional experimental approach. Journal of Structural Geology 14, 73–83.

March, A., 1932. Mathematische Theorie der Regelung nach der Korngestalt bei affiner Deformation. Zeitschrift fur Kristallographie 81, 285–297.

Marre, J., 1986. The Structural Analysis of Granitic Rocks. Elsevier, Oxford.

Mazzuchelli, M., Rivalenti, G., Piccirillo, E.M., Girardi, V.A.V., Civetta, L., Petrini, R., 1995. Petrology of the Proterozoic mafic dyke swarms of Uruguay and constraints on their mantle source composition. Precambrian Research 74, 177–194.

Oyhantçabal, P., Derregibus, M., Muzio, R., de Souza, S., Peel, E., 1993. Complejo Granítico Solís de Mataojo: evidencias de magmatismo sincolisional relacionado a subducción. Revista Brasileira de Geociências 23, 242–247.

Passchier, C.W., Trouw, R.A.J., 1996. Microtectonics. Springer, Berlin.

Preciozzi, F., Spoturno, J., Heinzen, W., 1979. Carta Geoestructural del Uruguay, escala 1:2.000.000. Instituto Geológico Eduardo Terra Arocena, Montevideo.

Ramberg, H., 1975. Particle paths, displacement and progressive strain applicable to rocks. Tectonophysics 28, 1–37.

Ramsay, J.G., 1980. Shear zone geometry: a review. Journal of Structural Geology 2, 83–89.

Ramsay, J.G., 1989. Emplacement kinematics of a granite diapir. The Chindamora batholith, Zimbabwe. Journal of Structural Geology 11, 191–210.

Ramsay, J.G., Huber, M., 1983. The techniques of Modern Structural Geology. Volume 1: Strain Analysis. Academic Press, London.

Schulmann, K., Jezek, J., Venera, Z., 1997. Perpendicular linear fabrics in granite: markers of combined simple shear and pure shear flows? In: Bouchez, J.L., Hutton, D.H.W., Stephens, W.E. (Eds.). Granite: from Segregation of Melt to Emplacement Fabrics. Kluwer Academic Publishers, Netherlands, pp. 158–170.

Truesdell, C., 1953. Two measures of vorticity. Journal of Rational Mechanics Analysis 2, 173–217.

Umpierre, M., Halpern, M., 1971. Edades Estroncio—Rubidio en rocas cristalinas del sur de la República Oriental del Uruguay. Revista de la Asociación Geológica Argentina 26, 133–151.

Vauchez, A., 1987. The development of discrete shear-zones in a granite: stress, strain and changes in deformation mechanisms. Tectonophysics 33, 137–156.

Willis, D.G., 1977. A kinematic model of preferred orientation. Bulletin of the Geological Society of America 88, 883–894.